Research Article Adv. Mat. Lett. 2012, **3**(3), 204-212 ADVANCED MATERIALS Letters

www.vbripress.com, www.amlett.com, DOI: 10.5185/amlett.2012.4332 Published online by the VBRI press in 2012

On lattice distortion by isovalent cations in silver sulphate solid electrolyte

S. W. Anwane

Department of Physics, Shri Shivaji Science College, Congress Nagar, Nagpur 440012, India

*Corresponding author. Tel: (+91) 712-2423432; Fax: (+91) 712-2440955; E-mail: swanwane2000@yahoo.com

Received: 14 April 2012, Revised: 15 May 2012 and Accepted: 18 May 2012

ABSTRACT

Detailed impedance spectroscopic studies are carried out by incorporating various guest iso-valent cations within the solid solubility limit having different ionic radii in Ag_2SO_4. The solid solubility limits up to x = 3 mole% cation doped Ag_2SO_4 are set with XRD, SEM, IR and DSC techniques. A major dependence of conductivity on the ionic size of the doped iso-valent cations is observed. The ionic conductivity is found to increase with the incorporation of a guest cation that creates *appropriate* distortion factor in iso-valent cation doped Ag_2SO_4. The conductivity of Ag_2SO_4 is found to be dependent on the ionic size of the guest cation, particularly in the low-temperature modification of Ag_2SO_4 (β-phase). These results could throw light on the fundamental conduction mechanism in Ag_2SO_4 and also on the criterion of selecting the impurity cation in the classical doping method. The optimized solid electrolytes can then be utilized for their technological applications in electrochemical devices such as SO_x sensors and thermal batteries. Copyright © 2012 VBRI Press.

Keywords: Lattice distortion; solid electrolytes; silver sulphate; fast ionic conductors.

S. W. Anwane obtained Ph.D. degree from Nagpur University in 2000 and is working as Associate Professor in Physics at Shri Shivaji Education Society Amravati's SCIENCE COLLEGE, Congress Nagar, Nagpur. He has worked on Fast Ionic Conductor, Solid Electrolytes, Gas Sensors, Simulation. He has published books on Applied Physics, Electromagnetic Fields. He is recipient of Senior Research Fellowship of Council of Scientific & Industrial Research, New Delhi..

Introduction

Silver sulphate, a non-alkali metal sulphate, is an exception which shows high cationic conductivity in spite of the bigger size of Ag^+. It undergoes a structural phase transition from the high temperature highly conducting hexagonal α-phase to the low temperature moderately conducting orthorhombic β-phase at 416°C. It attracted scant attention until its potential application in SO_x (x=2, 3) galvanic sensors was proved [**1**]. Recently, ever since the concept of using a metal/metal sulphate reference electrode in solid electrochemical gas sensors has evolved, it has attracted a great deal of attention. It exhibits many advantages over other sulphate-based [**2**] solid electrolytes in engineering SO_2 gas sensors like: (i) coexistence of Ag−O−S phase in Ag/Ag_2SO_4; (ii) equilibration of antagonist SO_4^{2-}(solid) with SO_2/SO_3 (gas); (iii) invariance of high ionic conductivity over the SO_x environment, etc. [**3-5**]. In contrast to earlier reports [**6**], our preliminary investigations revealed that in addition to valency, the ionic size and electronic structure of doped cations do play an important role in ion transport through the solid in low-temperature phases of sulphates [**7-12**]. The solid solubility limit for $(100\text{-}x)Ag_2SO_4$:$(x)Me_2SO_4$ has been established for $x \leq 3$mole% (Me=Li, Na, K, Rb & Cs). Variation in the parameters like peak frequency, pre-exponential factor, activation energy, ionic conductivity has been studied as a function of lattice distortion (contraction/expansion). The trend has been interpreted on the basis of structural changes caused in the host lattice of Ag_2SO_4 when Ag^+ is partially replaced by Li^+, Na^+, K^+, Rb^+ & Cs^+. The present work revisits [**8**] study on role of electronic structure and the influence of lattice distortion caused by iso-valent cations) on the mobility of Ag^+ in orthorhombic β-Ag_2SO_4 to understand the fundamental conduction mechanism and simultaneously to obtain an apt silver sulphate based material for SO_2 gas sensor. A detailed structural analysis based on XRD, SEM, IR confirms the solid solubility limits of the monovalent sulphates in the host β-Ag_2SO_4.

A fine analysis of lattice distortion has been carried out to understand its effect on conductivity of the newly synthesized solid electrolyte material. Comprehensive impedance analysis has been carried out to understand the lattice distortion contribution in governing conductivity and activation energy. Polynomial of 3rd order has been explored in governing role of factors expanding/contracting the lattice for its correlation with the conductivity and activation energy. Investigations on lattice distortion in superconducting phase/super ionic conductors have been explored by various workers [**13-15**].

Experimental

The initial ingredients Ag_2SO_4, Me_2SO_4 where Me=Li, Na, K, Rb, Cs; with assay more than 99.99% were procured from Aldrich Chemicals (USA). These pre-dried initial ingredients with mole fractions $(100-x)Ag_2SO_4$:$(x)Me_2SO_4$ (where x=0–7 mole%), were mixed in an agate mortar under acetone for 2 hrs. The compositions were filled in translucent quartz ampoules (to avoid photo decomposition of Ag_2SO_4) and were heated in an electric furnace to a temperature 20°C above the melting-point. Later, the melt was allowed to crystallize by cooling at a cooling rate of 1.5°C/min. The ingots, obtained by breaking the ampoules, were pulverized to get a fine powder.

The prepared samples were characterized by X-ray powder diffraction (XRD) (Philips PW1700 diffractometer attached with PW 1710 controlling unit) using CuK_α radiation. The solid–solid phase transition temperature and the heat of transition were studied by Differential Scanning Calorimetric (DSC) using Mettler TA 4000, DSC 25 at a heating rate of 10°C/min. The microstructures were examined with the help of Scanning Electron Microscope (SEM) (Cambridge 250 Mark-III stereoscan electron microscope). Using InfraRed (IR) spectroscopy, the stack plots of the samples were recorded in several spectral regions of interest using a Perkin-Elmer 983 IR spectrometer.

For electrical characterization, the specimens were obtained in the form of circular discs of 9mm diameter and 2mm thickness by pressing the powder with the help of a Specac (UK) stainless steel die-punch and hydraulic press. The pellets so obtained were sintered at 500°C for 24 hrs. Prior to spring loading of the pellets between silver electrodes, a good ohmic contact was ensured by using a quality silver paint on both opposite parallel surfaces of the pellet, followed by baking at 200°C for 2 hrs. Preceding the impedance measurement, the spring-loaded sample was heated to 510°C for an hour to homogenize the charge carriers in the sample and simultaneously to remove the moisture content therein. Later, the temperature of the furnace was reduced in step of 20°C at a cooling rate of 2°C/min. At the end of each cycle the sample was allowed to attain thermal equilibrium for a dwell time of 30 minutes using a Eurotherm 810 PID temperature controller. At the end of each dwell time, the real and imaginary parts of the impedance were measured as parametric functions of frequency in the range 5Hz–13MHz and temperatures from 510 to 100°C during the cooling cycle using an HP 4192A IF impedance analyzer. The entire measurement system was properly shielded to avoid external electrical pickups. A stainless steel faraday cage was employed for this purpose.
The ionic transference number of the specimens was measured by Wagner's dc polarization method using a Keithley SMU 236 with cell configuration: Ag/Electrolyte/Pt.

A small dc potential was applied across the above configuration to record current at zero and saturation time to know the current under polarized and un-polarized current to obtain the ionic transference number.

$$t_i = \frac{\sigma_0 - \sigma_\infty}{\sigma_0}$$

The reproducibility of the impedance data and transference number was confirmed by repeating the measurement on freshly prepared samples.

Results and discussion

Structural characterization forms the very basis for understanding the structure correlated conduction mechanism [**16-22**].

X-ray powder diffraction

The XRD pattern for all five systems was obtained at room temperature. Up to x=3 mole%, the lines corresponding to the guest cation are absent while a small intensity for Me_2SO_4 starts appearing for x > 3 mole% concentrations and above. This indicates that up to x=3 mole% Me forms solid solution with Ag_2SO_4. A comparison of experimental, d, and relative intensity values, I/I_0, with those of JCPDS data is given in **Table 1**.

Table 1. A comparison of experimental d and I/I_0 values with JCPDS data for (97)Ag_2SO_4:(3)Me_2SO_4 in orthorhombic phase.

Me=Li		Me=Na		Me=K		Me=Rb		Me=Cs		JCPDS data for Pure Ag_2SO_4		
d (Å)	I/I0	d (Å)	I/I0	d (Å)	I/I0	d (Å)	I/I0	d (Å)	I/I0	d (Å)	I/I0	[hkl]
4.694	7	4.702	8	4.697	8	4.698	7	-	-	4.699	10	[111]
3.987	20	3.995	11	3.950	19	3.955	20	-	-	3.994	25	[220]
3.171	59	3.171	29	3.177	71	3.178	68	3.177	59	3.177	70	[040]
2.871	101	2.873	100	2.876	100	2.875	100	2.878	100	2.873	100	[311]
2.642	48	2.648	31	2.645	54	2.646	54	2.647	55	2.644	90	[022]
2.415	23	2.481	12	2.421	25	2.421	24	2.425	32	2.421	30	[311]
1.926	17	1.923	18	1.926	24	1.927	26	-	-	1.926	30	[351]
1.708	14	1.713	8	1.710	20	1.711	19	-	-	1.712	17	[062]

It is clearly evident that in the case of 3mole% Me_2SO_4 added to Ag_2SO_4 the d values in XRD patterns are slightly deviated from the JCPDS data of β-Ag_2SO_4 (**Table 1**). This small deviation in experimental d(Å) values can be attributed to the partial replacement of Ag^+ by wrong-sized Me^+. Further, no decomposition appears from the XRD data. The absence of any line corresponding to either Me_2SO_4, $AgMeSO_4$ or any other intermediate phase for 3mole% Me_2SO_4 added to Ag_2SO_4 indicates solid solubility (SS). In case of (95) Ag_2SO_4:(5) Me_2SO_4 added to Ag_2SO_4, few meager lines corresponding to Me_2SO_4 appear which may be attributed to the advent of precipitation following its *in situ* dispersion in the host Ag_2SO_4 (SS). A closer look at **Table 1** reveals that, in general, there is a slight shift (negative) in d(Å) values for the systems where the dopant ion size is smaller than that of Ag^+, such as Li^+ and Na^+, whereas the shift is positive in d(Å) values for dopants with relatively bigger-size cations, such as K^+, Rb^+ and Cs^+. The local lattice distortion caused by the 'wrong'-size cation substitutions was further investigated to detect the magnitude of the distortion. This lattice distortion which has a primary indication of small shift in 'd' value has been further investigated to find the change in lattice volume and its effect on ionic conductivity.

A closer look at **Table 2** reveals that the cell volume undergoes a continuous contraction for Li^+ and Na^+; whereas it undergoes a continuous expansion for K^+, Rb^+ and Cs^+ substitution. These results (lattice contraction/expansion on the substitution of the smaller/bigger alio-valent cations (**Table 2**)) are suggestive of the fact that that lattice distortion (expansion and contraction) is directly governed by the 'distortion factor', R_g/R_h, R_g and R_h being the ionic radii of the guest and host cations, respectively. The lattice cell volume for $(97)Ag_2SO_4$:$(3)Me_2SO_4$ has been calculated and volume distortion factor V_g/V_h has been presented in **Table 2**. It clearly reveals that the ionic radius of smaller/grater size causes lattice contraction/expansion. Moreover, electro-negativity (according to Pauling) and outer electron shell is also displayed in the table for an overview.

System/Parameters		Me=Li	Me=Na	Me=Ag	Me=K	Me=Rb	Me=Cs
Lattice Parameters	*a*	10.221	10.227	10.269	10.271	10.241	10.267
	b	12.682	12.686	12.706	12.726	12.714	12.737
	c	5.753	5.75	5.818	5.823	5.853	5.841
Cell Volume		745.7195	746.0034	759.1205	761.1105	762.0844	763.8321
Ionic Radius R of cation (nm)		0.06	0.095	0.133	0.144	0.149	0.267
$\frac{R_g}{R_h}$		0.4511	0.7142	1.0000	1.0827	1.1203	2.0075
$\frac{V_g}{V_h}$		0.9823	0.9827	1.0000	1.0026	1.0039	10062
Electro-negativity (Pauling)		1	0.9	0.8	1.9	0.8	0.7
Outer Shell		$2s^1$	$3s^1$	$4s^1$	$5s^1$	$5s^1$	$6s^1$

Fig. 1 represents the variation of normalized volume distortion $\left(\frac{V_g}{V_h}-1\right)$ with normalized cation size $\left(\frac{R_g}{R_h}-1\right)$ which we shall call distortion coefficient. The trend of data points clearly indicates that as the size of guest cation (distortion coefficient) doped is increased/decreased the volume (normalized) accordingly increases/decreases. This can be clearly attributed to expansion and contraction of the lattice. Further second degree polynomial fit of the data points has been obtained to understand the non-linear behavior exhibited. The second degree polynomial fitted with R-squared value 0.888 governed by equation.

$$\left(\frac{V_g}{V_h}-1\right) = -0.017\left(\frac{R_g}{R_h}-1\right)^2 + 0.027\left(\frac{R_g}{R_h}-1\right) \ldots(1)$$

here in the given host silver sulphate lattice, the doping causing volume expansion is governed by coefficient 0.027 while the contraction by -0.017. The empirical formula (1) developed helps in interpolations/extrapolations over and around the data points. It possesses local maxima at (0.794, 0.0107).

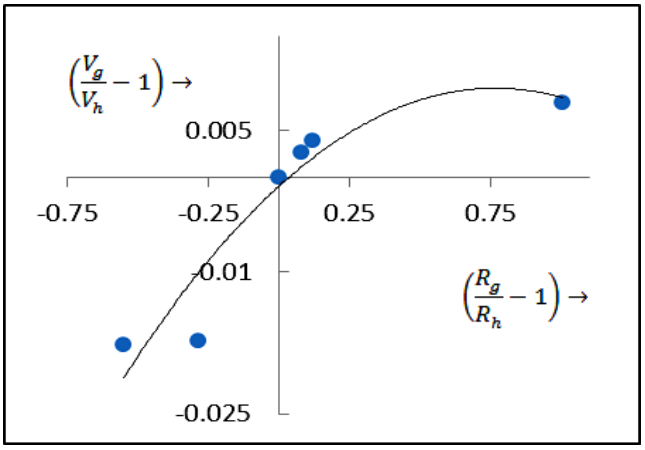

Fig. 1. Plot of normalized lattice distortion coefficient versus normalized volume distortion in Orthorhombic phase.

Differential scanning calorimetry (*DSC*)

Differential Scanning Calorimetric (DSC) and Infra Red (IR) studies were carried out on all samples. It was observed that for *x*=0, 0.5, 1, 3 mole % the DSC isotherms, transition temperature, enthalpy etc remained same. The Infra-red spectrums are also identical for *x*=0, 0.5, 1, 3 mole% leaving the frequency nodes unchanged. A DSC isotherm and IR spectrum for the sample *x*=0 are depicted in **Fig. 2**.

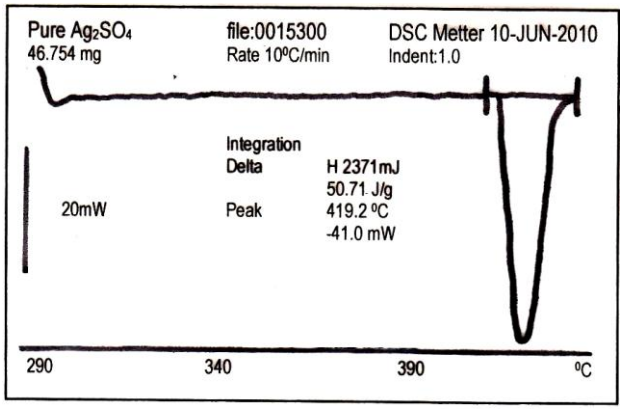

Fig. 2. DSC isotherm for pure Ag_2SO_4.

The phase transition temperature and heat of transition obtained from the thermograms of Me=Cs added samples has been presented in **Table 2**. It is evident from the **Table 2** that the transition temperature decreases like in many cases [**23-26**] with addition of impurity within solid solution region. Absence of additional peak in the thermogram indicates that no other phase is present.

Table 2. DSC Data for (100-*x*)Ag_2SO_4:(*x*)Cs_2SO_4.

Sample composition	J/gm	T ^oC
x=0	50.7	429.2
x =0.5	51.7	427.5
x =1	55.9	429.5
x =3	24.0	429.2
x =5	49.7	429.5

The decrease in phase transition temperature may be due to the partial replacement of host cation by the guest. Such partial replacement resulting due to the formation of solid solution that gives raise to additional strain energy caused by local elastic distortion. The additional strain energy is considered to be main factor responsible for promoting the solid-solid phase transition to occur at relatively lower temperature as compared to host system.

Table 3. Frequencies (cm^{-1}) for composition with small size and big size cation in Ag_2SO_4.

Wave No/ composition	Me=Li				Me=Rb		
	x=0	*x*=0.5	*x*=1	*x*=3	*x*=0.5	*x*=1	*x*=3
ν_1	98	98					
	3	0	980	981	984	987	989
ν_2	46	46					
	6	7	482	485	471	472	468
ν_3	11	11	111	112	112	112	112
	23	21	6	1	5	7	8
ν_4	61	61					
	9	7	617	618	618	617	620

Infrared spectroscopy (IR)

Various frequencies obtained from the infrared spectra of a number of compositions including that of pure Ag_2SO_4 are compared with the standard spectra of Ag_2SO_4 in **Table 3** to understand the role played by the impurity cation *vis-a-vis* the Ag_2SO_4 structure. **Fig. 3** indicates Infra-Red spectrum for pure Ag_2SO_4. **Table 3** indicates wave number and transmittance nodes. It clearly shows a negligible change for concentrations up to 3 mole %.

Table 3 shows the fundamental frequencies of SO_4^{2-} having T_d symmetry occurring at ν_1, ν_2, ν_3 and ν_4 respectively, the symmetric stretching (Raman active), doubly degenerate bending (IR active) and the doubly degenerate anti-symmetric (IR and Raman active frequencies)).

These frequencies are in closed agreement with the earlier reported [**27-28**] for SO_4^{2-} of Ag_2SO_4. Energy consideration (mainly electrostatic and thermodynamic) suggests the splitting of degenerate modes which depend on cations; it increases with increase in ionic radii, ionic polarizability and cation oxygen distance for isomorphous sulphate. No other additional frequencies other than those corresponding to Ag_2SO_4 are observed.

It rules out the possibility of precipitation or formation of intermediate phase. These results strongly support XRD results discussed in preceding sections. Moreover, it can be seen from the data that ν_1 and ν_3 shift to the lower values when Ag^+ is replaced by small size Li^+. On the other hand ν_1 and ν_3 shift to the higher values when Ag^+ is replaced by large size Rb^+.

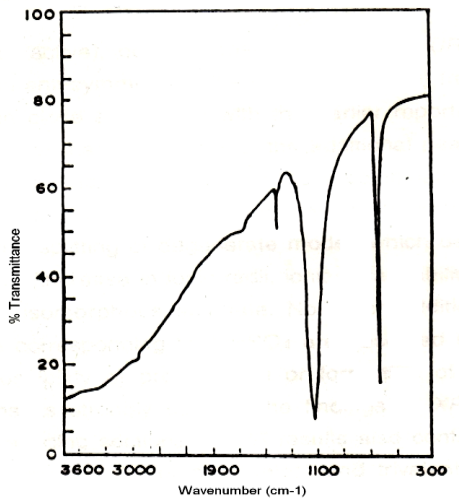

Fig. 3. Infra Red Spectrum for pure Ag_2SO_4.

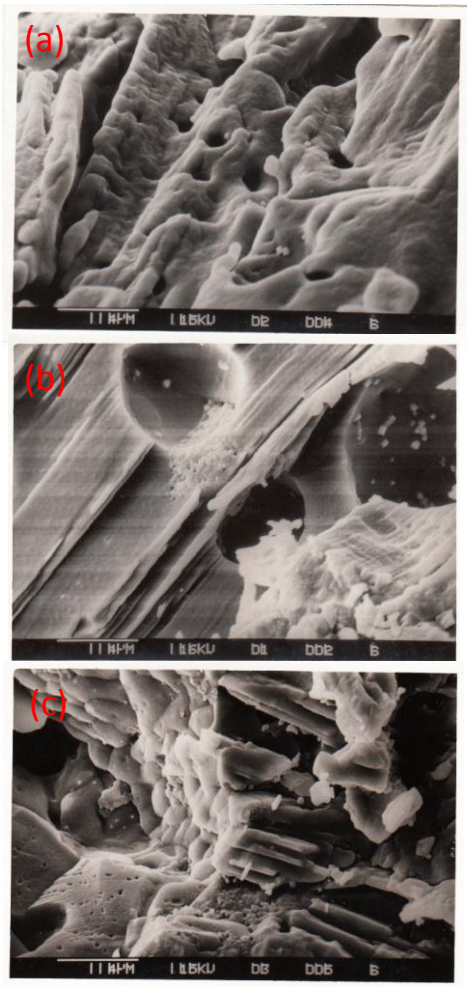

Fig. 4. Microphotographs of (100-*x*)Ag_2SO_4:(*x*)Rb_2SO_4 with (*a*) *x*=0, (*b*) *x*=3 and (*c*) *x*=5 mole%.

Scanning electron microscopy (SEM)

The formation of solid solubility of various cations in Ag_2SO_4 is further confirmed by the evidences obtained by characterizing the samples using SEM. **Fig. 4** representing microphotographs of (100-*x*)Ag_2SO_4:(*x*)Rb_2SO_4 with (a) *x*=0, (b) *x*=3 and (c) *x*=5 mole% reveals that the grain morphology of the host material is more or less unaffected by an addition up to *x*=3 of Rb_2SO_4. On the other hand, a few traces of insoluble Rb_2SO_4 are visible in **Fig. 4(*c*)** for samples with *x*=5. Similar results are found in other monovalent systems. These results suggest that a complete solid solution can be ensured only up to 3 mole% of Me_2SO_4 in room temperature orthorhombic phase.

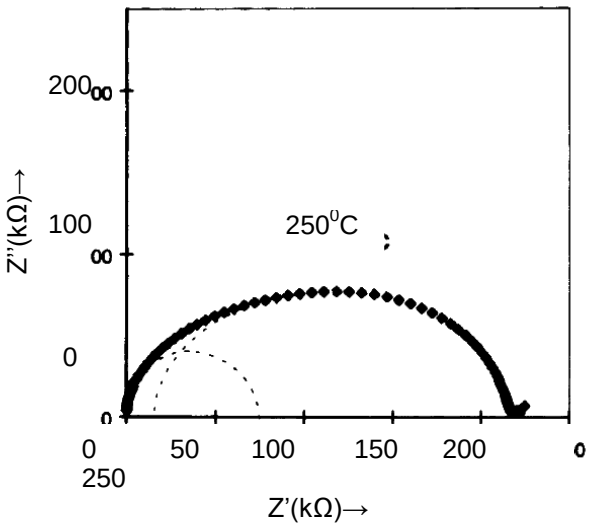

Fig. 5. Complex impedance plot for pure Ag_2SO_4 at 250 °C (the doted line represents the best fit curve)

Impedance analysis

The results of complex impedance spectroscopy are critically analyzed to find bulk properties by eliminating extraneous parameters such as electrode polarization and grain boundary. A distorted semicircular arc is observed for the pure sample (**Fig. 5**). A closer look at this figure reveals that the distorted semicircular arc is a combination of two overlapping depressed semicircular arcs. On the other hand, a single semicircular arc is seen for K^+, Rb^+ and Cs^+ which is attributed to the limitation of the upper sweep frequency (13MHz). However, there are two discernible semicircular arcs in the case of the rest of the samples.

Since the conductive silver coating on both the surfaces of the electrolyte acts as a reversible (non-blocking) electrode, no electrode polarization is reflected in the complex impedance plane. A non-linear least squares (NLS) fit method is used to ascertain the presence of two overlapping depressed semicircular arcs. In order to accomplish this, the complex impedance data acquired at a fixed temperature using a computer controlled HP 4192A IF impedance analyzer is fitted to the following equation using our software developed in Turbo C.

$$Z = Z(0) + \frac{Z(\infty)-Z(0)}{1+(j\omega\tau)^{\alpha}} \qquad \ldots(2)$$

where $Z(0)$ and $Z(\infty)$ are limiting values of $Z(\omega)$ when ω varies from minimum to maximum, τ is relaxation time, α is empirical measure of departure from ideal Debye model. During the NLS fitting the sum of squares is minimized by unity weighting represented by

$$S_i = (\Delta R_i)^2 + (\Delta I_i)^2 \qquad \ldots(3)$$

where ΔR_i and ΔI_i are the real and imaginary fitting residuals. The presence of two overlapping depressed semicircular arcs is suggestive of the occurrence of two prominent conduction mechanisms simultaneously under the external perturbation ac signal. Various interpretations can be made in the impedance analysis in a polycrystalline ion conducting specimen; however, an experimental impedance obviously contains major contributions from inter-grain and intra-grain ion migration [**29-30**]. In order to have a more meaningful discussion, the voluminous impedance data obtained by following the above procedure are fitted in using the equation

$$f_p = f_0 e^{\frac{-E_m}{kT}} \qquad \ldots(4)$$

The peak frequency of the complex impedance

$$\omega_{max} = 2\pi f_p$$
$$\frac{1}{\tau} = \frac{1}{RC} = \frac{\sigma}{\varepsilon\alpha\mu C}. \quad \mu = \mu_0 e^{\frac{-E_m}{kT}} \qquad \ldots(5)$$

where μ is the cationic mobility, E_m denotes the migration enthalpy, μ_0 is proportional to the jump attempt frequency, and *k* and *T* are the Boltzmann constant and temperature in *K*. The frequency *f*p derived from ω_{max} is an effective averaged hopping frequency of an ion. The effective pre-factor f_0 depends on the defect charge carrier density, *C*.

The process of ion migration through the sample involves the activation energy for migration of ions across the grain boundaries, E_{a2} (obtained from the semicircle corresponding to high frequency) and that for migration of ions within grain (intra-grain) ion migration, E_{a1} (obtained from the semicircle corresponding to low frequency). Evidently, the partial replacement of the host Ag^+ by dopant cations within the grain alters the local environment leaving the grain boundary undisturbed. This alteration in the local environment modifies the activation enthalpy for intra-grain ion migration, whereas that for inter-grain conduction remains invariant. Similar results are found in case of the iso-valent cation doped Li_2SO_4 [**31**].

In the complex impedance plot real and imaginary impedance has been plotted as a parametric function of frequency. It indicates a depressed semicircular arc and for the series of interest the peak frequency has been plotted with relative ionic radius. It also exhibits a trendy behavior as shown in **Fig. 6**.

The given data points for relative ionic radius with f_p has been least square fit to third degree polynomial with R-squared value 0.998;

$$f_p = 3392\left(\frac{R_g}{R_h}\right)^3 - 5957\left(\frac{R_g}{R_h}\right)^2 - 3819\left(\frac{R_g}{R_h}\right) + 9744 \qquad \ldots(6)$$

The R-squared value 0.998 confirms third degree polynomial Eq (6) encompasses trend of data points in the **Fig.6** which reveals the peak frequency in complex impedance plot also depend upon the distortion coefficient $\left(\frac{R_g}{R_h}\right)$. The coefficients arising in the equation are governing lattice distortion factors supporting and opposing ion migration that varies with the lattice expansion and contraction.

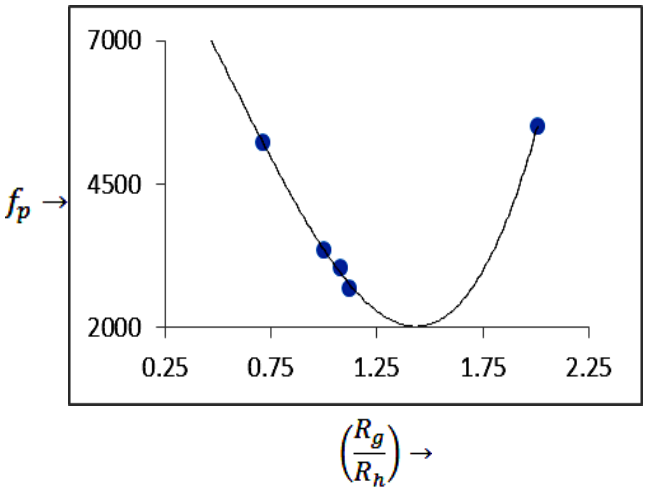

Fig. 6. Plot of relative ionic radius versus f_p.

Ionic conductivity

The generalized perception of Arrhenius theory of the temperature effect on the reaction rate (ion diffusion) originated from the temperature effect on the equilibrium constant. It is known that:

$$\frac{dln(K)}{d\frac{1}{T}} = -\frac{H}{R} \qquad \ldots(7)$$

where K is an equilibrium constant, R is the gas constant, and H is the heat of reaction. The equilibrium constant is $= \frac{k_1}{k_2}$, where k_1 and k_1 are the rate constants for the forward and reverse reactions respectively. Thus, we obtain;

$$\frac{dln(k_1)}{d\frac{1}{T}} - \frac{dln(k_2)}{d\frac{1}{T}} = -\frac{H}{R} \qquad \ldots(8)$$

Arrhenius recognized that the last equation could be conveniently divided into two parts, each having the form of:

$$\frac{dln(k)}{d\frac{1}{T}} = -\frac{E}{R} \qquad \ldots(9)$$

where E is referred by Arrhenius as representing the energy difference between the reactants and an activated species. The term E is, therefore, called the activation energy. Taking E as a constant the last can be integrated to yield:

$$ln(k) = ln(A) - \frac{E}{RT}$$

where $ln(A)$ is the constant of integration and the last equation can be converted to:

$$k = Ae^{-\frac{E}{RT}} \qquad \ldots(10)$$

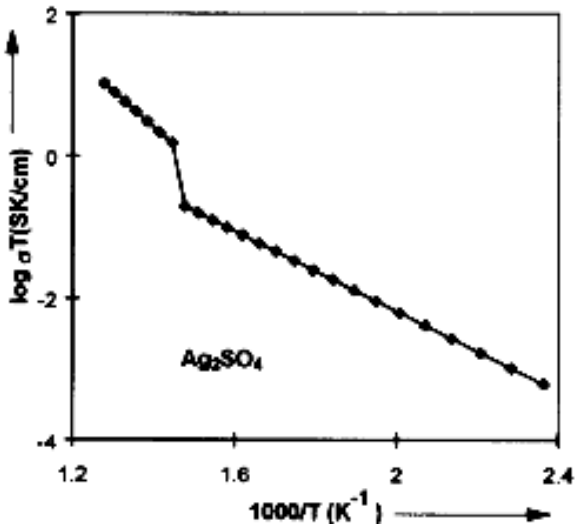

Fig. 7. Arrhenius plot for pure Ag_2SO_4 in α and β phases.

This form of equation (10) is the most widely adopted form of the Arrhenius equation. The temperature dependent ionic conductivity in all specimens is governed by Arrhenius equation can be expressed as equation (11);

$$(\sigma T) = (\sigma T)_o exp\left(\frac{E_a}{2KT}\right) \qquad \ldots(11)$$

The pre-exponential factor $(\sigma T)_o$ in the above equation (which is appearing out of constant of integration) is related to the frequency of ionic collisions in the collision theory and to the entropy term in the transition state theory. The equation governs forward and reverse reaction contributing to ionic conductivity (σT) and predomination of each other. Arrhenius plots for all the compositions are found to obey the Arrhenius law (11) in both the α and β phases (as an example, **Fig. 7** depicts this behaviour for the host Ag_2SO_4).

The observed change in slope at 416°C with an order of magnitude jump in conductivity in the case of pure Ag_2SO_4 accounts for the orthorhombic β to hexagonal α phase transition (**Fig. 5**). The magnitudes of the conductivities (2.22×10^{-5} S/cm at 250°C and 3.4×10^{-3} S/cm at 440°C) and the transition temperature (416°C) are in close agreement with earlier reports [**32-35**].

Concentration dependent conductivity

The concentration of mobile charge carriers in a Frenkel type ionic solid is given by

$$n = \sqrt{k_f}\ exp\left(\frac{\Delta S_{th} + \Delta S_{cf}}{2k} - \frac{E_f}{kT}\right) \qquad \ldots(12)$$

where k_f, ΔS_{th}, ΔS_{cf} and E_f are, respectively, the mass action constant, thermal entropy, configurational entropy and defect formation enthalpy. If the system under consideration (solid solution of Ag_2SO_4 with Me_2SO_4) is assumed to be homogeneous and isotropic, then the term ΔS_{cf} remains invariant with respect to the distribution of cations and anions, whereas the immediate ions surrounding Me^+ will have a different vibrational frequency (ν') from those at regular undistorted sites ν. The thermal entropy term, ΔS_{th} in the last equation will be a consequence of the change in frequency of the lattice vibration due to the distortion taking place. Considering the Einstein model we may assume that in the doped crystal, each atom neighboring Me^+ is equivalent to three harmonic oscillators each of frequency $\nu' \neq \nu$. Then one finds for the increase in thermal entropy per Me^+ the expression,

$$\Delta S_{th} = 12klog\left(\frac{\nu}{\nu'}\right) \quad \ldots(13)$$

substitution of which in last equation (12) leads to:

$$n = k_f \left(\frac{\nu}{\nu'}\right)^6 exp\left(-\frac{E_f}{2kT}\right) \quad \ldots(14)$$

This reduces the mobile charge carrier (Ag^+) concentration, *n*. This is reflected in the conductivity behaviour (a decrease in conductivity) in the cases of Na^+ and Li^+ doped samples (Fig. 8c). The opposite behaviour is expected if $R_g > R_h$ in which case lattice loosening occurs. Such an expansion opens the lattice in the vicinity of Me^+ thereby widening the window (opening) between the two energetically equivalent cationic sites through which the ion undergoes successive jumps from an occupied site to the vacant site. Cs^+ has $R_g \gg R_h$ such that the lattice undergoes expansion but beyond a critical value, the wrong-sized dopant ion hinders the mobility of Ag^+, thus reducing the conductivity (**Fig. 8c**).

Nevertheless, in the case of Li_2SO_4 added to Ag_2SO_4, in spite of the lattice contraction the lattice opening of the host is large enough for the added Li^+ that it itself can move from one site to a nearby vacant site, i.e., the added Li^+ becomes the mobile charge carrier.

Additionally, coupling of Ag^+–Li^+ helps in the enhancement of the conductivity; the net effect is such that in spite of the lattice contraction, in the case of Li^+ doped Ag_2SO_4, the conductivity is marginally enhanced. The observed insignificant decrease in conductivity (Na^+ doped Ag_2SO_4) is understandable because with the addition of Na^+ the total mobile charge carrier density remains the same. A small decrease in conductivity due to partial replacement of Ag^+ by Na^+ has also been observed by Secco et al [**36-40**]. Rb^+ cation causes optimum lattice expansion that offers optimum ionic conductivity.

Lattice distortion dependent conductivity

As seen in **Fig. 8a** and **b**, the conductivity is optimized in the β- and α-phases for *x* = 3mole% in the case of Li, Na, K, Rb and Cs doping, whereas the conductivity is found to decrease slightly with concentration for Na doped Ag_2SO_4. The Cs^+ doping decreases the conductivity in β -Ag_2SO_4. A closer look at the figure clearly reveals that the Rb^+ doped sample gives the maximum conductivity in both phases. Interestingly, the Li^+ doped samples have conductivities comparable to that of the pure host system. When Ag^+ is partially substituted by Me^+, a lattice distortion (increased entropy) occurs, in general, affecting the mobility of the cation in the host lattice. Particularly, a localized lattice contraction takes place if $R_g < R_h$ (such as Na^+ and Li^+ replacing Ag^+), and the lattice expands if $R_g > R_h$ (such as K^+, Rb^+ or Cs^+ replacing Ag^+) as substantiated by the experimental facts.

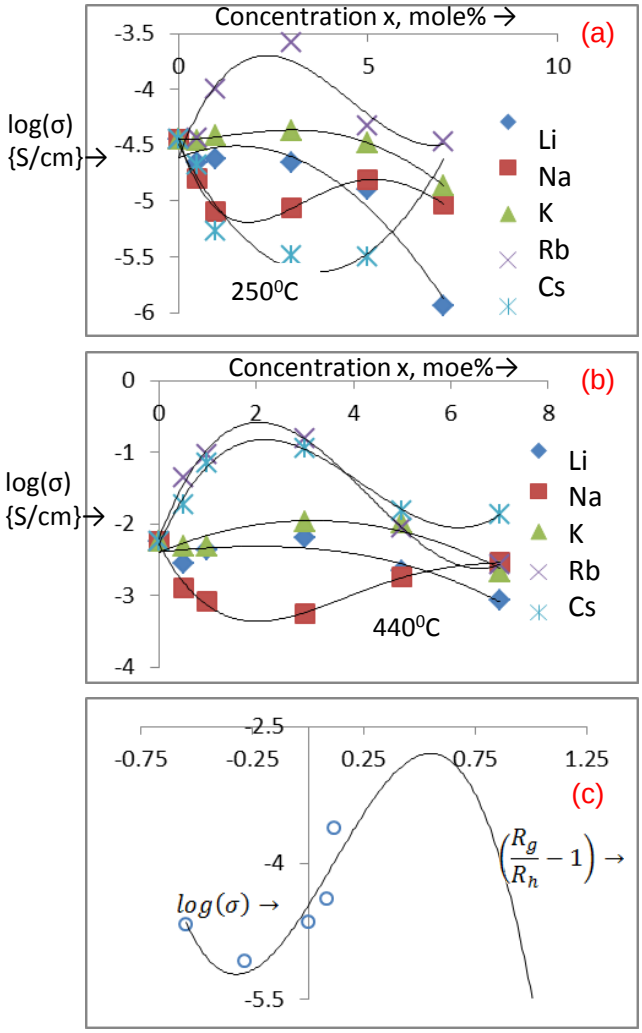

Fig. 8. Variation of log(σ) with *x* for (100-*x*)Ag_2SO_4:(x)Me_2SO_4 [Me=Li, Na, K, Rb, Cs] at (a) 250°C, (b) 440°C, (c) with normalized lattice distortion.

The variation of ionic conductivity of (97)Ag_2SO_4:(3)Me_2SO_4 for Me=Li, Na, Ag, K, Rb and Cs has been plotted as a function of lattice distortion factor $\left(\frac{R_g}{R_h} - 1\right)$. The way lattice volume has undergone a trendy contraction and expansion, conductivity has also undergone a trendy change. This change has been least square fit with third

degree polynomial as depicted below with R-squared value 0.881.

$$log(\sigma) = -7.358\left(\frac{R_g}{R_h} - 1\right)^3 + 2.488\left(\frac{R_g}{R_h} - 1\right)^2 + 3.902\left(\frac{R_g}{R_h} - 1\right) - 4.469 \quad \ldots(15)$$

The empirical formula (15) developed helps in interpolations/extrapolations over and around the data points. It possesses local maxima at (0.548,-2.79).

This pre-exponent appearing in the equation has been calculated for all system and for $97Ag_2SO_4{:}3Me_2SO_4$ it has been studied as it how relates to lattice distortion. The trend of the pre exponential factor with relative lattice volume has been depicted in **Fig. 9**.

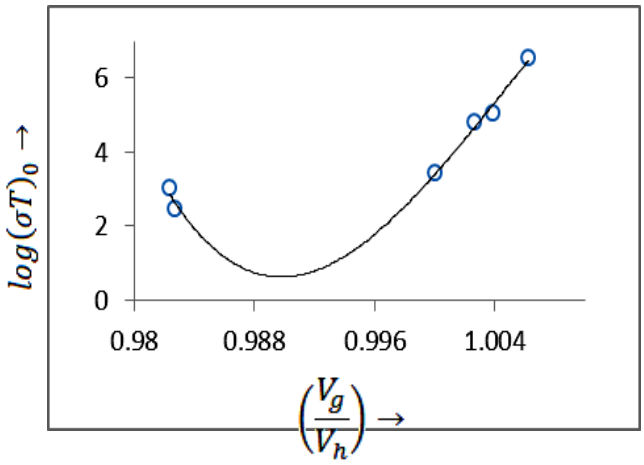

Fig. 9. Plot of relative lattice volume versus $\log(\sigma T)_0$.

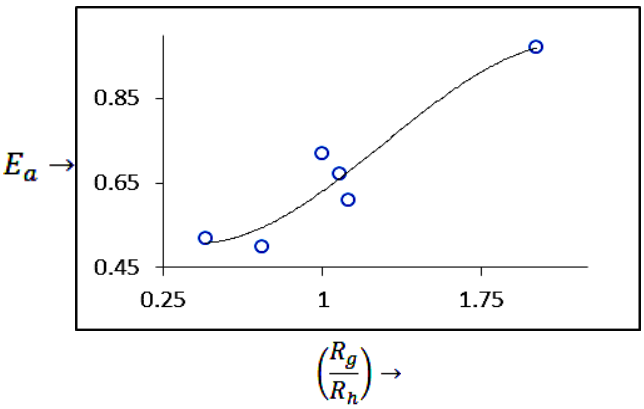

Fig. 10. Relative ionic radii vs. activation energy.

A third degree polynomial is fitted in the given data quite accurately that the R-squared value is 0.986 i.e. close to 1. The polynomial has been found as;

$$log(\sigma T)_o = -79703\left(\frac{V_g}{V_h}\right)^3 + 2 \times 10^6\left(\frac{V_g}{V_h}\right)^2 - 2 \times 10^6\left(\frac{V_g}{V_h}\right) + 80684 \quad \ldots(16)$$

The activation energy (**Fig. 10**) which is superposition of forward and reverse reaction of ion migration through lattice for the series of interest has been studied as a function of relative ionic size of doped cation. The relative ionic size with activation energy has trend of non-linear increase as size of doped cation increased. The third degree polynomial least square fitting for R-squared value 0.901 is;

$$E_a = -0.177\left(\frac{R_g}{R_h}\right)^3 + 0.685\left(\frac{R_g}{R_h}\right)^2 - 0.478\left(\frac{R_g}{R_h}\right) + 0.601 \quad \ldots(17)$$

The empirical formula can be utilized to interpolate and extrapolate the effect relative lattice volume on the pre-exponential factor and provides lattice coefficients arising due to lattice distortion factors on the pre-exponential factor. In the lattice contraction region the curve has negative slope while in lattice expansion it possesses positive slope but with having minima at $\left(\frac{V_g}{V_h}\right) = 0.989$.

Conclusion

The ionic conductivity is found to increase with the incorporation of a guest cation that creates *appropriate* distortion factor, $\left(\frac{R_g}{R_h}\right)$, in iso-valent cation doped Ag_2SO_4. The increase in conductivity in the doped Ag_2SO_4, despite having $R_g < R_h$, is due to the probable role played by the lattice distortion. The conductivity of Ag_2SO_4 is found to be dependent on lattice distortion caused by the ionic size of the guest cation, particularly in the low-temperature modification of Ag_2SO_4 (β-phase). The optimum conductivity is obtained for x=3 mole% which forms solid solution of Li, Na, K, Rb & Cs in host Ag_2SO_4. The pre-exponential factor, conductivity, activation energy, peak frequency has been optimized with lattice distortion factor caused by mis-match of ionic radius. An empirical equation for optimization using non-linear-least square fit method has also been obtained to understand the trend for generalization. These results could throw light on the fundamental conduction mechanism in Ag_2SO_4 and also on the criterion of selecting the impurity cation in the classical doping method. The optimized solid electrolytes can then be utilized for their technological applications in electrochemical devices such as SO_x sensors and thermal batteries.

References

1. Gauthier M; Chamberland A *J. Electrochem. Soc.* **1977** 124, 1579. **DOI:** 10.1149/1.2133114
2. Ramaswamy V; Vimalathithan R M; Ponnusamy V *Adv. Mat. Lett.* **2012**, 3(1), 29-33 **DOI:** 10.5185/amlett.2011.4240
3. Liu H Y; Hupp J T; Michael J. *Weave J. of Electroanal Chemy & Interfacial Electrochem* **1984** 179, 1-2, 219. **DOI:** 10.1016/S0022-0728(84)80290-9
4. Liu S H; Hinnen C; Huong C; Tacconi N R; Hoa K M; *J of Electroanalytical Chem & Interfacial Electrochem* **1984** 176, 1–2, 325. **DOI:** 10.1016/S0022-0728(84)80327-7

5. Mari, C.M.; Beghi, M; Pizrini, S. *Sensors and Actuators B*, 1990, 2, 51-55. **DOI:** 10.1016/0925-4005(90)80008-N
6. Hofer H H; Eysel W; Alpen U V *J. Solid State Chem.* **1981** 36, 365. **DOI:** 10.1016/0022-4596(81)90448-5
7. Singh K; Bhoga S S *Solid State Ionics* **1990** 39, 205. **DOI:** 10.1016/0167-2738(96)00120-8,
8. Singh K; Anwane S W; Bhoga S S *Solid State Ionics* **1996** 86-87, 187. **DOI:** 10.1016/0167-2738(96)00120-8
9. Singh K; Pande S M; Anwane S W; Bhoga S S *J. App. Phy. A* **1998** 66, 205. **DOI:** 10.1007/s003390050657
10. Singh K; Pande S M; Bhoga S S *Bull Mater Sci* **1995** 19(3) 237. **DOI**: http://www.ias.ac.in/jarch/bms/18/00000246.pdf
11. Nandi S; Kim M G, Kreyssig; Fernandes R M; Pratt D K *Phys Rev Lett* **2010** 104. **DOI:** 10.1103/PhysRevLett.104.057006
12. Stingl C; Perry R S; Maeno Y;Genenwart P *Phys Rev Lett* **2011** 107. **DOI:** 10.1103/PhysRevLett.107.026404
13. Singh K; Pande S M; Anwane S W; Bhoga S S *Bulletin of Electrochemistry* **1996** 12 (11-12) 625. **DOI:** 10.1007/BF02745557
14. Anwane S W; Anwane R S *Adv. Mat. Lett.* **2012**, 3(2), xxx. **DOI:** 10.5185/amlett.2012.1314
15. Singh K *Solid State Ionics* **1988** 28, 1371. **DOI:** 10.1016/0167-2738(88)90389-X
16. Yeh N C; Fu C C; Wei J Y T; Vasquez R P; Huynh J; Maurer S M; Beach G; Beam D A *J. Appl. Phys.* **1997** 81, 5499. **DOI:** 10.1063/1.364580
17. Jin S; Tiefel T H; McCormack M; Fastnacht R A; Ramesh R; Chen L H *Appl. Phys. Lett.* **1995** 66, 382. **DOI:** 10.1063/1.114220
18. Hwang H Y; Cheong S W; Radaelli P G; Marezio M; Batlogg B *Phys. Rev. Lett.***1995** 75, 914. **DOI:** 10.1103/PhysRevLett.75.914
19. Moritomo Y; Asamitsa A; Tokura Y; *Phys. Rev. B* **1995** 51, 16 491. **DOI:** 10.1103/PhysRevB.51.16491
20. Khazeni K; Jia Y X; Lu L; Crespi V H; Cohen M L; Zettl A, *Phys. Rev. Lett.* **1996** 76, 2, 295. **DOI:** 10.1103/PhysRevLett.76.295
21. Ibarra M R; Algarabel P A; Marquina C; Blasco J; Garcia, J. *Phys. Rev. Lett.* **1995** 75, 3541. **DOI:** 10.1103/PhysRevLett.75.3541
22. Zhao G M; Conder K; Keller H; Muller K.A. *Nature* **1996,** *381*, 676. **DOI:** 10.1038/381676a0
23. Kimura; Greenblatt *Mat Res Bull* **1984** 19, 1553. **DOI:** 10.1016/0025-5408(84)90243-5
24. Gopalan G P; Kulkarni A R *J Solid State Chemistry* **1998** *138(2)*, 183. **DOI:** 10.1006/jssc.1998.7770
25. Murray R M; Secco E A *Can J Chem* **1978** 56, 2616. **DOI:** 10.1139/v78-430
26. Singh K; Bhoga S S *Solid State Ionics* **1990** 39, 205. **DOI:** 10.1016/0167-2738(90)90399-C
27. Yang, P.H.; Yang, J.H.; Chen, C.S.; Peng, D.K.; Meng, G.Y.; *Solid State Ionics* **1996**, 86-88, 1095. **DOI**: 10.1016/0167-2738(96)00275-5
28. Meloche V W; Kalbus G E *J. Inorg Nucl Chem* **1958** 6, 104 **DOI:** 10.1016/0022-1902(58)80054-8
29. Singh K *Solid State Ionics* **1993** 66, 5. **DOI:** 10.1016/0167-2738(93)90021-T
30. Muccilloa ENS; Kleitzb M *Journal of the European Ceramic Society* **1996** 16(4) 453. **DOI:**10.1016/0955-2219(95)00125-5
31. Bhoga S S; Singh K; *Ionics* **2007** 13,6, 417. **DOI:** 10.1007/s11581-007-0150-7
32. Liu Q; Worrel W L *Solid State Ionics* **1988** 28-30(2) 1668. **DOI**: 10.1016/0167-2738(88)90439-0
33. Weppner W *Solid State Ionics* **1981** 3(4) 1. **DOI**:10.1016/0167-2738(81)90044-8 12
34. Weppner, W *Solid State Ionics* **1981** 5 (3). **DOI**: 10.1016/0167-2738(81)90186-713
35. Weppner W *Sens & Actu* **1987** 12(2) 107. **DOI**: 10.1016/0250-6874(87)85010-2
36. Yan Y; Miura N; Yamazoe N *Sens & Actu B*: *Chem* **1995** 24, 1(3) 287. **DOI**: 10.1016/0925-4005(95)85062-7
37. Secco E A; Usha M G *Solid State Ionics* **1994** 68, 213. **DOI**:http://dx.doi.org/10.1016/0167-2738(94)90178-3
38. Liaw B Y; Liu J; Menne A; Weppner W *Solid State Ionics* **1992** 53–56(1) 18. **DOI**: 10.1016/0167-2738(92)90359-W
39. Suganuma S; Watanabe M; Kobayashi T S; Wakabayashi *Solid State Ionics* **1999** 126 (2) 175. **DOI**: 10.1016/S0167-2738(99)00220-9
40. Benzinger W; Wenka A; Dittmeyer R *Applied Catalysis A 2011: General* **2011**397, 1(2) 209. **DOI**: 10.1016/j.apcata.2011.03.001

